Design of MPPT DC-DC Converter Fed Ripple Switch Inductor Quasi-ZSI with Different Control Methods For Renewable Energy Application

Sarbojit Mukherjee, MIEEE[1], Chandan Mal[2], Ghanshyam Yadav[3]

***Corresponding Author: -** Sarbojit Mukherjee, MIEEE
Address:*[1]Department of Electrical Engineering RCC Institute of Information Technology Kolkata, West-Bengal, NDIA
sarbo.1234@gmail.com
[2]Department of Electrical Engineering RCC Institute of Information Technology Kolkata, West-Bengal, INDIA
chandanmal77@gmail.com
[3]Department of Electrical Engineering RCC Institute of Information Technology Kolkata, West-Bengal, INDIA
gsyadav1233@gmail.com
Sarbojit Mukherjee, Mieee, Chandan Mal,Ghanshyam Yadav, Design Of Mppt Dc-Dc Converter Fed Ripple Switch Inductor Quasi-Zsi With Different Control Methods For Renewable Energy Application

Abstract:
In this paper, a two-stage renewable energy conversion system, consisting of boost dc-dc converter and a Ripple Switch Inductor Z-Source Inverter (rSL-qZSI), is proposed. In recent years, besides Voltage Source Inverter and Current Source Inverter, Quasi ZSI (qZSI) is getting focused because of having low device specifications for middle and high-power range applications. An Incremental Conductance (IC) based Maximum Power Point Tracking (MPPT) technique is used to develop the Pulse Width Modulated (PWM) signal for basic boost dc-dc converter for extraction of maximum Solar Photo-Voltaic (SPV) power in variable ambient conditions. Further a rSL-qZSI is used which has high voltage boosting capability and low switching device voltage stress compare to other conventional qZSI. Two different control methods, i.e. Maximum Boost Control (MBC) and Third Harmonic Injection (THI) control, are applied to boost the output voltage. In this paper operating principle, analysis and design of both dc-dc converter and rSL-qZSI has been done. A comparative analysis has been shown between these control methods for different modulation index. To verify the performance of the proposed topology, a MATLAB simulation model has been designed. The implementation of MPPT along with the rSL-qZSI voltage boosting behavior has been verified through the simulation results.

Keywords: Ripple SL-qZSI, MPPT, Maximum Boost Control (MBC), Third harmonic injection (THI) control.
DOI Number: 10.14704/nq.2022.20.9.NQ44547 **Neuro Quantology 2022; 20(9):4715-4726**

1. Introduction

Renewable energy is a kind of natural energy, which is unlimited in nature and available freely. Solar energy is one kind of renewable energy that can replace fossil energy such as coal, crude oil, etc. India lies on the Tropic of Cancer, which provides large solar energy. Conventionally a photovoltaic system is required to improve solar energy, and it has some advantages such as being environment-friendly and low maintenance cost [1]. The main disadvantage of PV is that it requires a high installation cost and low efficiency. Characters like irradiance, temperature, dirt, shadow and sunlight spectral effects the efficiency of the solar cell. Change in temperature and irradiance, due to different type of weather, reduce the Solar Photo Voltaic (SPV) output. Different researchers proposed different Maximum Power Point Tracking (MPPT) techniques for maximum power extraction from the SPV, improving the efficiency all over the system.

In the conventional system, a DC-DC converter, which behaves as an interface between SPV and load, is used to transfer power to the load. Different isolated[2], non-isolated[3], [4], buck [5], boost[6] and buck-boost [7], [8]converter with variable duty cycle is used to extract maximum power from SPV. The maximum Power carries out by the DC - DC convertor from the PV to the load by adjusting duty cycle and when load changes, DC-DC convertor distribute the maximum power.

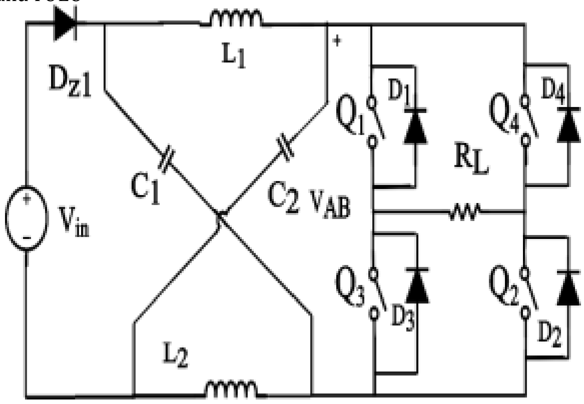

Fig. 1. Basic Z-Source Inverter

A general Z-Source Inverter (ZSI) structure is shown in the Fig. 1. As shown in the Fig.1 a two-port unique impedance network, consist of a cross shape connected split inductors (L_1 and L_2) and capacitors (C_1 and C_2), employed between the dc power supply and the main inverter circuit. Compare to the conventional Voltage Source Inverter (VSI), where six active states and two zero states are observed, ZSI has an extra shoot through state. Shoot-through state can be generated by different ways. Presence of this shoot through state in ZSI established a unique buck-boost feature into it. But more losses along with increasing unreliability may cause for classical ZSI with higher boosting operation.

In recent years, several ZSI topologies are proposed by different researcher. If modelling, controls and modulation techniques are prioritized by few and some researchers are focused to developed new topologies. The distortion in the output waveforms is significantly reduced with increased reliability as dead time switching is eliminated for Quasi- Z Source Inverter (q-ZSI) operation. Fig. 2(a) represents the basic structure of q-ZSI [9] which is nothing but some small modification of conventional ZSI. Similarly in Fig 2(c), an extended Z Source Inverter (EZSI) is proposed [10] where the primary dc source is divided into two part and connected accordingly. Improved input characteristics along with lower component specification for same power rating can be achieved in this topology. In [11], addition of several passive component, like inductor, capacitor and diode, to the conventional ZSI structure is proposed in order to enhance the boosting factor. As shown in the Fig. 2(c) and Fig 2(d), a Continuous-current diode assisted first extension boost Quasi-ZSI (DA-qZSI) and Continuous-current capacitor assisted first extension boost Quasi-ZSI (CA-qZSI) are proposed in [12]. In [13], a trans ZSI is proposed where Z-networked inductors are replaced by a 2:1 turns ratio transformer which enhanced the overall gain of the network. As shown in the Fig. 2 (e) a switched inductor structure is added with ZSI, named as switched-inductor ZSI (SL-ZSI), is proposed in [12] which eliminates the boost limitation of the conventional ZSI. Further with a small modification of SL-ZSI, a rippled input current Quasi-Z Source Inverter (rSL-qZSI) is developed where high gain can be achieved.

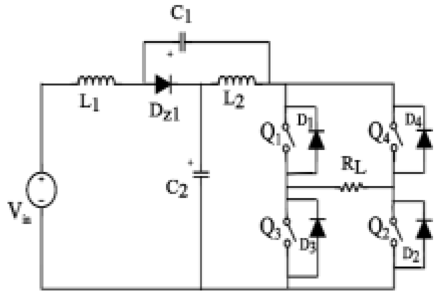

Fig 2. (a)

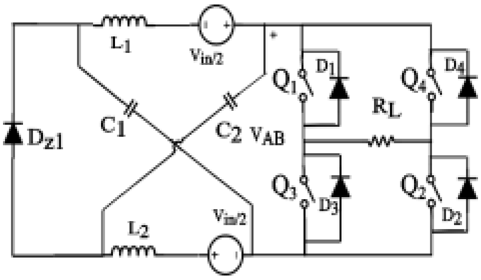

Fig 2. (b)

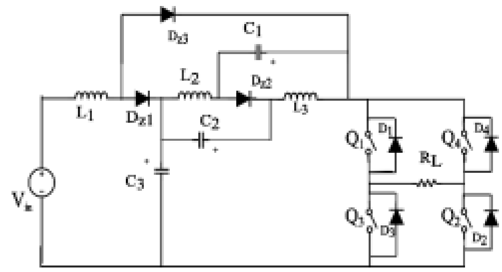

Fig 2. (c)

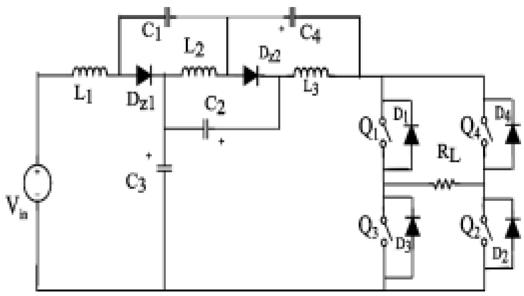

Fig 2. (d)

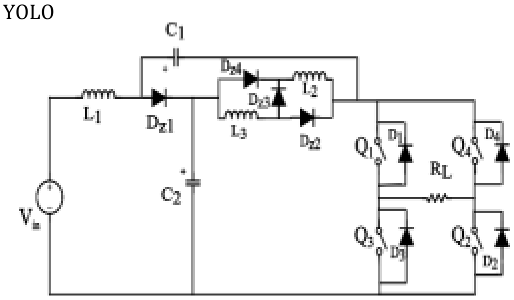

Fig 2. (e)

Fig 2. (a) Basic qZSI with continuous input current. (b) EZSI with continuous input current. (c) Continuous-current first extension DA-qZSI. (d) Continuous-current first extension CA-qZSI. (e) SL-ZSI structure.

In this paper, a MPPT dc-dc boost converter fed rSL-qZSI is proposed. Two different control methods, i.e., MBC and THI control, are used to enhance the efficiency of the system. The rest of the article is organized as follows: In the next section, named as proposed topology, explain the total proposed topology. Next section which is termed as operating principle, represents the operation of IC based MPPT, dc-dc boost converter and rSl-qZSI. In the next section, the control design for the qZSI is explained. In the later section, simulation results of different power characteristics along with multiple control are represented. In the final section the total study is concluded and a comparison of the proposed rSL-qZSI with other conventional ZSI is also represented.

2. Proposed Topology:

As shown in the Fig. 3 the overall structure of SPV-MPPT based rSL-qZSI with different modulation techniques is demonstrated. The whole configuration can be divided into two primary stages. First stage where a dc -dc boost converter is designed to extract maximum power from the SPV panel and produce a high voltage dc output.

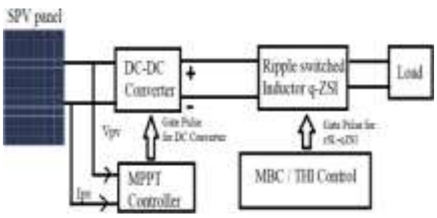

Fig. 3. Overall diagram of Proposed Topology

As, the SPV has a low output voltage, dc-dc boost converter used to boost it. Whereas in the second stage a rSL-qZSI is implemented for development of single-phase ac with further boosting factor. Along with this different control methods, such as MBC and THI control, are used to further boost the output voltage and improved the efficiency of the system.

3. Operating Principle:

A. SPV-MPPT system:

Photovoltaic system is a system that converts the solar energy taken from the environment to DC power. A PV is characterized by its open circuit voltage (V_{OC}), short circuit current (I_{sc}), maximum voltage (V_{max}) and maximum power point (MPP) current. Those parameters shape the I-V and P-V characteristic curve. The PV itself is a nonlinear system and can be defined as a variable current source which represented as

$$I_D = I_{OS}\left(e^{\left[\frac{q(V+R_sI)}{kT}\right]} - 1\right) \quad (1)$$

$$I_{OS} = I_{or}\left(\frac{T}{T_r}\right)^3 e^{\left[\frac{qE_{GO}}{\beta k}\left(\frac{1}{T_r}-\frac{1}{T}\right)\right]} \quad (2)$$

Where, I and V are the output current and output voltage of solar cell, I_{os} is diode's reverse saturation current, T is temperature in Kelvin, K is Boltzmann constant (1,381e-23 J/K), q is electric charge, I_{sc} is short circuit current at temperature of 25°C, Tr is reference temperature (298.18K) and I is saturation current at Tr. Current output also is influenced by diode's ideality factor and the range is between 1 and 2.

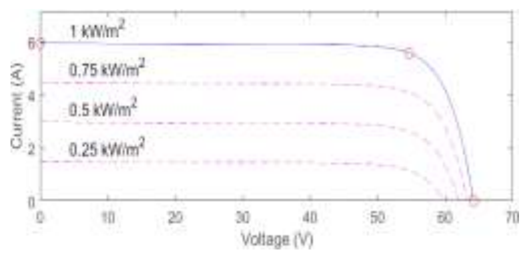

Fig 4. (a)

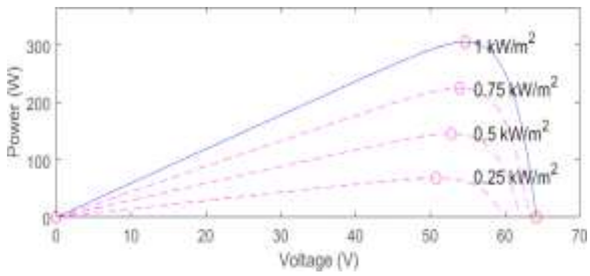

Fig 4. (b)

Fig. 4. (a) V-I characteristics of SPV panel. (b) P-V characteristics of SPV panel.

As the output power of the SPV is dependent on atmospheric condition like solar irradiance and temperature, as shown in Fig. 4, a tracking algorithm need to be implemented for extraction of maximum power from the SPV, generally named as MPPT. MPPT stands for Maximum Power Point Tracking is a technique which is used to maximize the energy connected to the solar module at any time during the operation. In different time, different MPPT algorithms are prescribed by multiple researchers [14], where Perturb and observe (P and O)[15], Incremental Conductance (IC) [16] fuzzy-MPPT [17] and Particle Swarm Optimization (PSO) -MPPT [18] techniques are famous. IC based MPPT methods are implemented in this proposed topology for its simplicity. The operation of the IC-MPPT algorithm is demonstrated in Fig. 5. IC will try to improve the tracking time by comparing the difference between dI/dV and –I/V. If dP/dV is negative then MPP will lies on the right side of the recent position and if dP/dV is positive then MPP will present on left side. The equation of IC method is

$$\frac{dP}{dV} = \frac{d(V.I)}{dV} = I + V\frac{dI}{dV} \quad (3)$$

When dP/dV=0 then MPP is reached and

$$\frac{dI}{dV} = -\frac{I}{V} \quad (4)$$

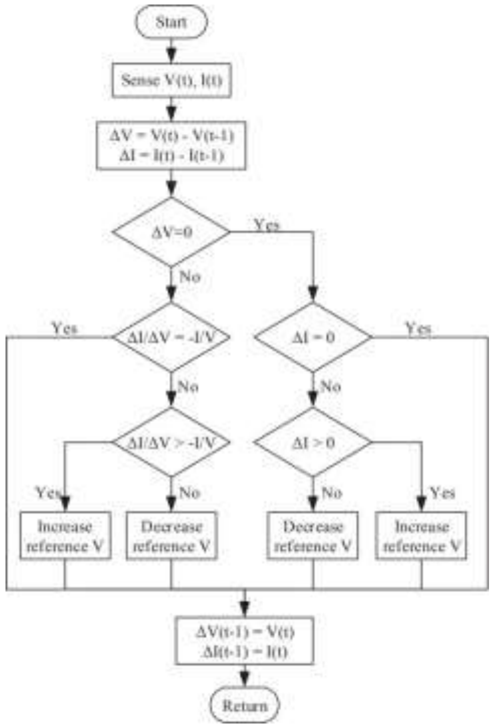

Fig. 5. Flowchart of Incremental Conductance based MPPT method.

If MPP lies on the right side then (dI/dV) < (-I/V) and PV voltage will be decreased to reach the MPP. IC method can be used for finding the MPP, improve the PV efficiency, it also reduces the power losses and cost of the system. The oscillation around MPP area can also be suppressed in trade of with its implementation complexity.

B. DC – DC Boost Converter

As described earlier, the output of the SPV will vary depending upon the ambience condition, generally a dc converter is used to implement MPPT. Besides that, the conventional SPV output terminal voltage is low which may not be suitable for different applications. So, a simple dc boost converter is used here [19]. The basic configuration of dc boost converter is shown in Fig. (a) which consist of an inductor (L), full controlled switch (Q) and a diode (D). Output capacitance and load resistance is represented by Co and Ro.

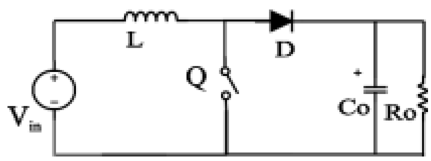

Fig 6. (a)

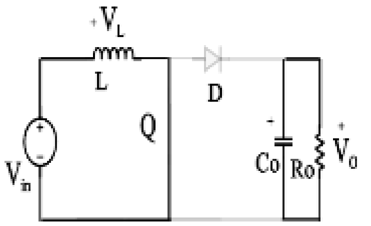

Fig 6. (b)

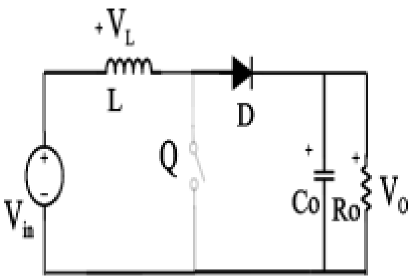

Fig 6. (c)

Fig. 6. (a) Basic Boost converter. (b) Operation of Boost converter when Q turned on. (c) Operation of Boost converter when Q turned off.

When the switch gets on, the diode becomes reverse biased thus, isolating the load stage. The input energy stores in the inductor. Once the power switch is off, the load stage gets energies from the inductor as well as from the input source, therefore the voltage across the load is greater than the source voltage. Further the operation of this converter is demonstrated in Fig. 6(b) and (c). The output voltage is expressed as

$$V_O = \frac{V_{in}}{1-D} \quad (5)$$

Where, D represents the duty cycle. V_{in} represent the supply input voltage. The value of the inductor (L) and capacitor (Co) can be designed using equation 6 and 7.

$$L = \frac{V_{in}D}{f_s \Delta I_O} \quad (6)$$

$$C = \frac{I_O D}{f_s \Delta V_O} \quad (7)$$

Where, f_s represented the switching frequency, ΔV_O and ΔI_O represent the ripple in output voltage and current respectively.

C. Ripple switched-inductor quasi-Z-source inverter

In the Fig. 7, ripple switched inductor quasi-Z-Source inverter is shown. This topology is derived from the SL-qZSI with a modification of the dc source position. Instead of connecting the dc source in the middle of the two switched inductor cell, as connected in SL-qZSI, dc source is connected in series with two switched cell(L_1 - L_2 - D_{Z2} - D_{Z3} - D_{Z4} or L_3 - L_4 - D_{Z5} - D_{Z6} - D_{Z7}). Because of this constructional modification, a small ripple emerges on the input current, for which this topology sometime named as rSL-qZSI. This topology can successfully minimize the initial inrush current compare to SL-qZSI. Besides that, a reduced voltage stress across the capacitor, dc source common ground sharing and having relatively flat shape input current are some of the advantageous features of this topology.

Generally, the operation of the conventional qZSI can be divided into six active and two zero states. Here in this topology an additional shoot through zero state is observed. So, operation of this topology is similar with the operation observed in ZSI and SI-ZSI. For simplified operation analysis the topology is divided in shoot-through and non-shoot-through states.

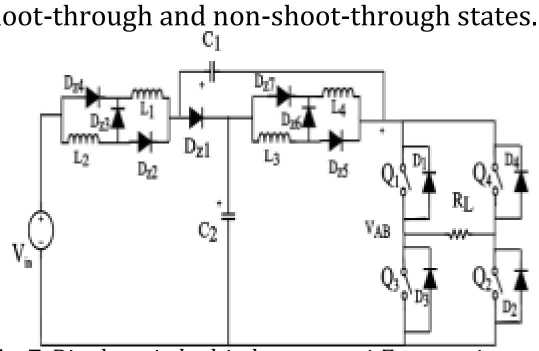

Fig. 7. Ripple switched-inductor quasi-Z-source inverter circuit

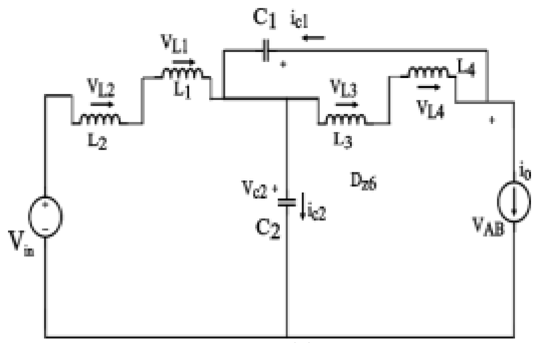

Fig 7. (a)

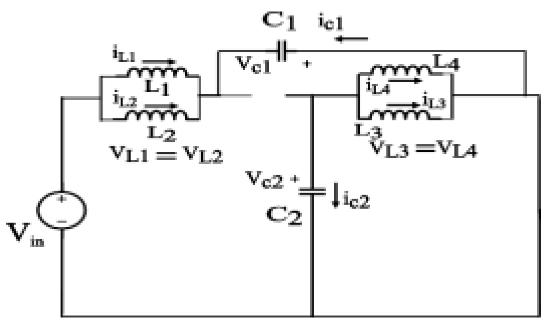

Fig 7. (b)

Fig.7. (a) Operating circuit in non-shoot-through mode
(b) Operating circuit in shoot-through mode

Fig.7 (a) and (b), represents the non-shoot-through and shoot-through states of the circuit. As shown in the Fig. 7(a) in the non-shoot-through mode main circuit draws a constant current, denoted by i_i, from the source. The diodes D_{Z1}, D_{Z3} and D_{Z6} are forward biased and remaining diodes D_{Z2}, D_{Z4}, D_{Z5} and D_{Z7} are reversed biased. Energy transfer from the supply dc (V_{in}) to the main circuit by the inductors L_1, L_2, L_3 and L_4 and capacitors, C_1 and C_2 are getting charged. V_{L1_NS}, V_{L2_NS}, V_{L3_NS} and V_{L4_NS} represents the non-shoot-through mode voltage across the inductors L_1, L_2, L_3 and L_4 respectively. The equation of the inductor voltages can be represented by

$$V_{L1} = V_{L1\_NS} = V_{C2} - V_{in} - V_{L3\_NS} \quad (8)$$

$$V_{L2} = V_{L2\_NS} = V_{C2} - V_{in} - V_{L1\_NS} \quad (9)$$

$$V_{L3} = V_{L3\_NS} = V_{C1} - V_{L4\_NS} \quad (10)$$

$$V_{L4} = V_{L4\_NS} = V_{C1} - V_{L3\_NS} \quad (11)$$

Where V_{C1} and V_{C2} represents the voltage across the capacitor C_1 and C_2 respectively. DC link voltage V_{AB} can be represented as

$$V_{AB} = V_{C1} + V_{C2} \quad (12)$$

Capacitor current can be given by,

$$i_{C1} = I_{L2} - i_O = I_{L4} - i_O \quad (13)$$

$$i_{C2} = I_{L2} - i_O = I_{L1} - i_O \quad (14)$$

In the shoot-through states, as shown in the Fig. 7(b), terminal voltage V_{AB} become zero as both switch in one of the legs becomes turned on. Diodes D_{Z1}, D_{Z3} and D_{Z6} are turned off, as they are reversed biased, and D_{Z2}, D_{Z4}, D_{Z5} and D_{Z7} turned on. Because of that, inductors L_1, and L_2 connected in parallel same as L_3 and L_4. All four-inductor stored energy and capacitor C_1 and C_2 discharged. The inductor voltages can be obtained as

$$V_{L1} = V_{L2} = -V_{C1} - V_{in} \quad (15)$$

$$V_{L3} = V_{L4} = -V_{C2} \quad (16)$$

The capacitors current can be represented by

$$i_{C1} = -I_{L2} - I_{L1} \quad (17)$$

$$i_{C2} = -I_{L3} - I_{L4} \quad (18)$$

After applying the volt-second balance equation across the inductor and capacitors,

$$V_{L1\_NS} = V_{C2} - \frac{D}{1-D} V_{C1} - \frac{1}{1-D} V_{in} \quad (19)$$

$$V_{L2\_NS} = V_{C2} - \frac{D}{1-D} V_{C1} - \frac{1}{1-D} V_{in} \quad (20)$$

$$V_{L3\_NS} = V_{L4\_NS} = \frac{-D}{1-D} V_{C2} + V_{C1} \quad (21)$$

$$I_L = I_{L1} = I_{L2} = I_{L3} = I_{L4} = \frac{1-D}{1-3D} i_o \quad (22)$$

$$I_{in} = (1+D) I_{L1} = \frac{1-D^2}{1-3D} i_i \quad (23)$$

Where, I_{in} represents the input average current of the rSL-qZSI. Substituting the values from the equation (8) - (14) to (19) to (23) capacitor voltages can be obtained as

$$V_{C1} = \frac{2D}{1-3D} V_{in} \quad (24)$$

$$V_{C2} = \frac{1-D}{1-3D} V_{in} \quad (25)$$

The expression of dc-link peak voltage can be calculated as

$$V_{AB} = V_{C2} + V_{C2} = \frac{1-D}{1-3D} V_{in} = BV_{in} \quad (26)$$

Where, B stand for the boost factor, can be expressed as

$$B = \frac{1-D}{1-3D} \quad (27)$$

The variation of the boost factor for different duty cycle can be shown in Fig. 8.

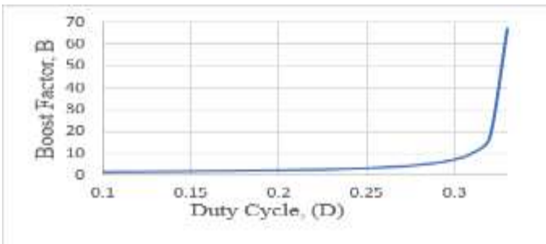

Fig. 8. Relation between Boost factor Vs Duty Cycle

4. Control for the rSL-q-ZSI:

4720

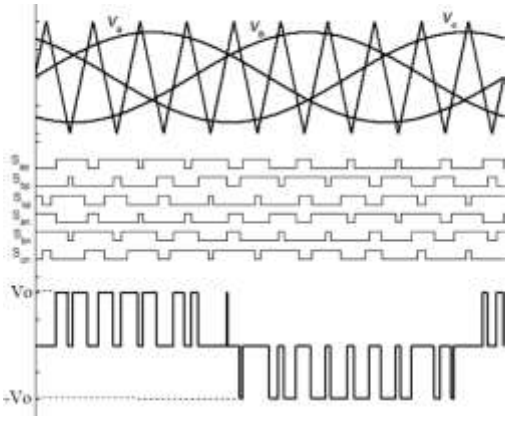

(a)

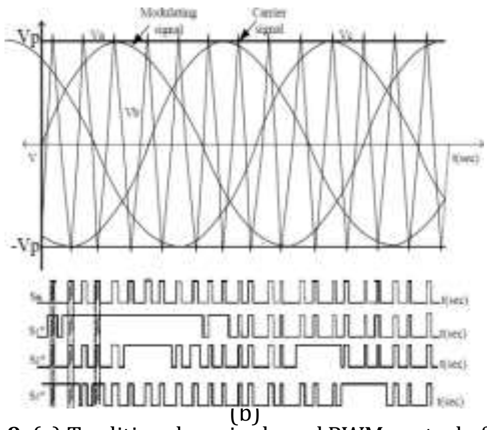

(b)

Fig. 9. (a) Traditional carrier based PWM control of ZSI
(b) Simple boost control method of ZSI

Fig. 9(a) represents traditional carrier based PWM control method where required PWM signal is developed by comparing a high frequency carrier signal with a sinusoidal wave. Conventional q-ZSI can be controlled by simple, maximum and constant PWM based boost control method. As explained in this [20], [21], in order to develop shoot through states, three phase references are compared with a fixed magnitude. The control of the duty cycle (D) can be modified as constant in the shoot through state. As shown in the Fig. 9(b). In simple boost control method, the maximum value of the duty cycle can be represented as

$$D = (1 - M) \qquad (28)$$

Where, M denotes the modulation index. So, from the equation (27) the equivalent boost factor can be represented by

$$B = \frac{2-M}{3M-2} \qquad (29)$$

The phase voltage peak voltage can be represented by

$$\hat{V}_{ph} = \frac{MV_{AB}}{2} = \frac{MBV_{in}}{2} \qquad (30)$$

A. Maximum Boost Control:

Disadvantage of Simple boost control, like more shoot through loss and decreasing shoot through duty ratio with increasing modulation index, can be overcome with maximum Boost Control (MBC) method. As shown in the Fig 10(a), the shoot through state will developed by comparing the carrier waveforms with maximum and minimum value of the modulating wave. In this method as the boost factor is maximum the output voltage is also maximum. Besides that, more switching loss can be observed as one of the disadvantages of this method.

As observed in Fig 10(a), the shoot through states repeats periodically every $\frac{\pi}{3}$. Assuming very high frequency switching compared to modulating frequency with an interval $(\frac{\pi}{6}, \frac{\pi}{2})$, the average shoot through duty ratio can be expressed as

$$\frac{T_o(\theta)}{T} = \frac{2-(M\sin\theta - M\sin(\theta - \frac{2\pi}{3}))}{2} \qquad (31)$$

$$\frac{\bar{T_o}}{T} = \frac{\int_{\frac{\pi}{6}}^{\frac{\pi}{2}} 2d\theta - \left(\int_{\frac{\pi}{6}}^{\frac{\pi}{2}} M\sin\theta d\theta - \int_{\frac{\pi}{6}}^{\frac{\pi}{2}} M\sin(\theta - \frac{2\pi}{3})d\theta\right)}{\int_{\frac{\pi}{6}}^{\frac{\pi}{2}} 2d\theta} \qquad (32)$$

$$\frac{\bar{T_o}}{T} = \frac{2\pi - 3\sqrt{3}M}{2\pi} \qquad (33)$$

Further the boost factor B can be expressed as

$$B = \frac{1}{1-2\frac{T_o}{T}} = \frac{\pi}{3\sqrt{3}M - \pi} \qquad (34)$$

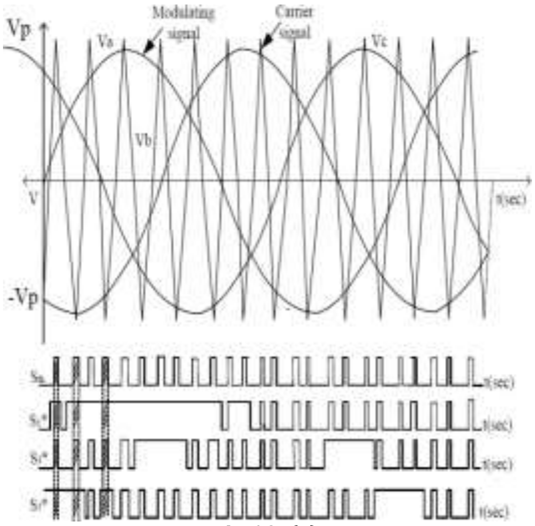

Fig 10. (a)

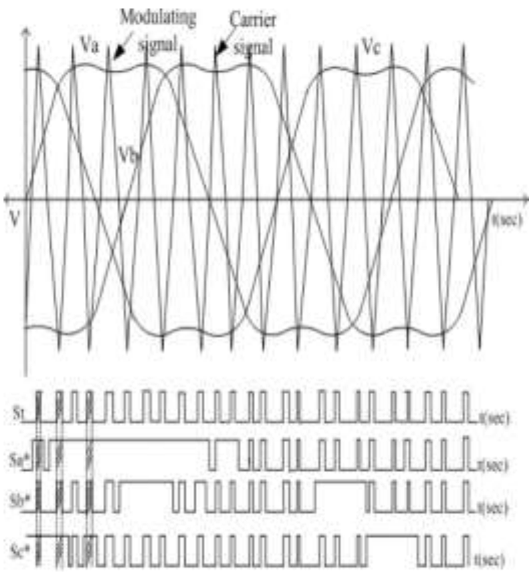

Fig 10. (b)

Fig. 10. (a) PWM generation for Maximum Boost Control (MBC) (b) MBC with third harmonic injection

B. Maximum Boost Control with Third Harmonic Injection:

In this method, the operation is almost same as maximum boost control except the modulating signal is modified by third harmonic injection. Fig 10(b) represents the operation of MBC with third harmonic injection. An additional 15% voltage boost can be achieved for similar V_{in}. Assuming similar shoot through repeating period and switching period interval the average shoot through duty ratio can be calculated

$$\frac{T_o(\theta)}{T}=\frac{2-(M\sin\theta+\frac{1}{6}M\sin 3\theta-(M\sin(\theta-\frac{2\pi}{3})+\frac{1}{6}M\sin 3\theta))}{2} \quad (35)$$

$$\frac{\bar{T_o}}{T}=\frac{\int_{\frac{\pi}{6}}^{\frac{\pi}{2}}2d\theta-(\int_{\frac{\pi}{6}}^{\frac{\pi}{2}}(M\sin\theta+\frac{1}{6}M\sin 3\theta)d\theta-\int_{\frac{\pi}{6}}^{\frac{\pi}{2}}(M\sin(\theta-\frac{2\pi}{3})+\frac{1}{6}M\sin 3\theta)d\theta)}{\int_{\frac{\pi}{6}}^{\frac{\pi}{2}}2d\theta} \quad (36)$$

$$\frac{\bar{T_o}}{T}=\frac{2\pi-3\sqrt{3}M}{2\pi} \quad (37)$$

Further the boost factor B can be expressed as

$$B=\frac{1}{1-2\frac{T_o}{T}}=\frac{\pi}{3\sqrt{3}M-\pi} \quad (38)$$

5. Simulation Results:

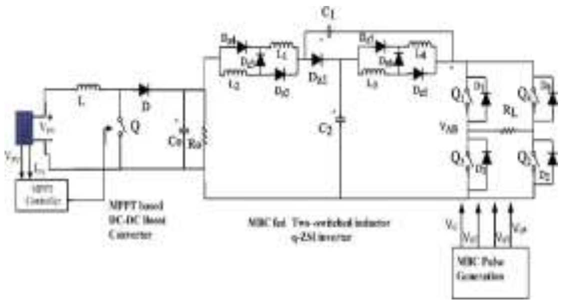

Fig. 11. Simulation diagram of Total circuit

As shown in the Fig. 11, based on the proposed topology a simulation circuit is created in MATLAB software. Verification of dc-dc converter behavior and different control characteristics of ripple SL-qZSI is done. Details specification of different power circuit component is given in the table-1. For this design a SPV panel (A10 Green Tech, Model: A10J-S72-175) with power rating of 175W, with V_{mpp} and I_{mpp} of 36.6V and 4.78A, is used. The successful implementation of IC based MPPT tracking operation id verified and shown in Fig. 12. A variation of irradiance is introduced (1000 W/m^2 to 500 W/m^2 to 800 W/m^2), indifferent time and variation of maximum power SPV power extraction (175W to 83W to 141W) is observed.

Table-1 Component Specification

eISSN 1303-5150

	Name	Rating
Solar PV Panel (A10 Green Tech) Model : A10J-S72-175	Input Panel Power	175W
	Open circuit Voltage (V_{oc})	43.99V
	The voltage at MPP (V_{mpp})	36.63V
	Short Circuit Current (I_{sc})	5.17A
	Current at MPP (I_{mpp})	4.78A
	Temp Coefficient of (V_{oc})	-0.3616 (%/deg C)
	Temp Coefficient of (I_{sc})	0.0415 (%/deg C)
Boost Converter	Inductor L	2.1mH
	Capacitor C_o	220μF
	Resistance R_o	80Ω
	Switching Frequency	5kHz
Ripple SL-qZSI-Converter	Inductor L_1, L_2, L_3 and L_4	300 μH
	Capacitor C_1 and C_2	470 mF
	Output Filter Inductor	1mH
	Output Filter Inductor	470 μF
	Load Resistance (R_L)	50 Ω
	Switching Frequency	10kHz

An 175W DC-DC boost converter is also designed with the specification given in table-1. This boost converter succesfully boost the input SPV panel voltage from 36.6V to 130V as shown in Fig. 15. A Pulse Width Modulated (PWM) signal, dc -dc converter switching, of 5 kHz is developed by the MPPT controller as shown in Fig. 16. A output voltage of 130V, with ripple of 6.15%, and output current of 1.3A,with a ripple 4.61%, are observed as shown in Fig. 16.

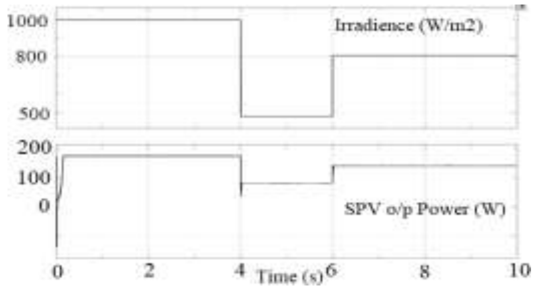

Fig. 12. MPPT tracking with variable irradience.

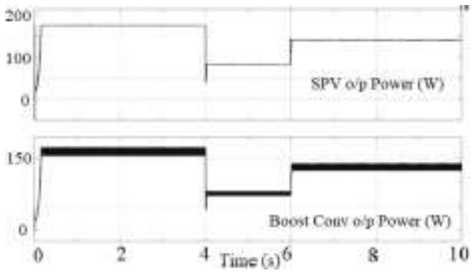

Fig. 13.SPV and Boost DC converter output power

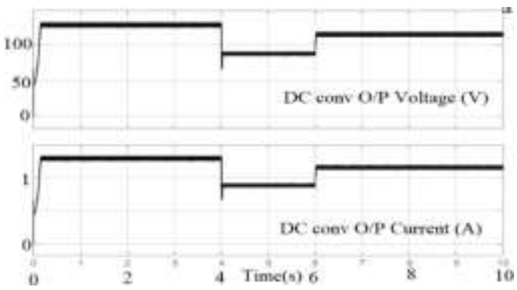

Fig. 14 DC-DC converter output voltage and current with gate pulse.

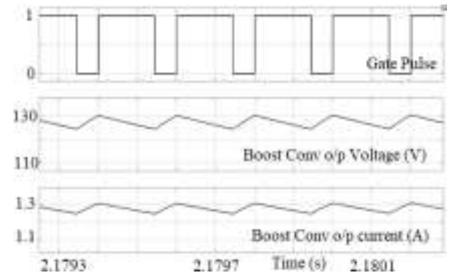

Fig. 15. Charging and discharging of dc converter with irradience variation.

In the Fig. 16, the load voltage and current for ripple SL-qZSI with Maximum Boost Control (MBC) for modulation index 0.7 is shown. A voltage of 90V with 0.9Amp current are observed. Besides that, voltage and current across the switch is represented in Fig. 21. As shown in Fig. 17, inductor current with peak value 4.6A with 25% ripple is observed. The voltage across the cpacitor (C_1) is near 140V with very minimal amount of ripple.

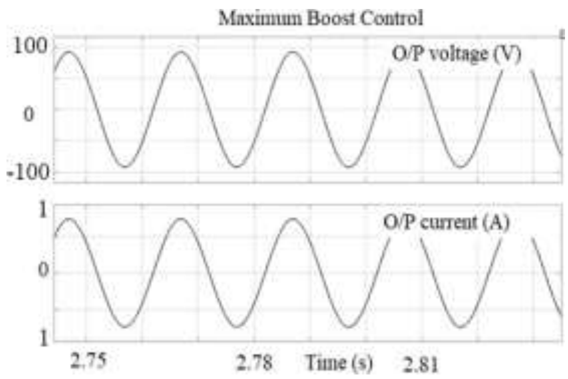

Fig. 16. Load voltage and current for MBC-ripple SL-qZSI

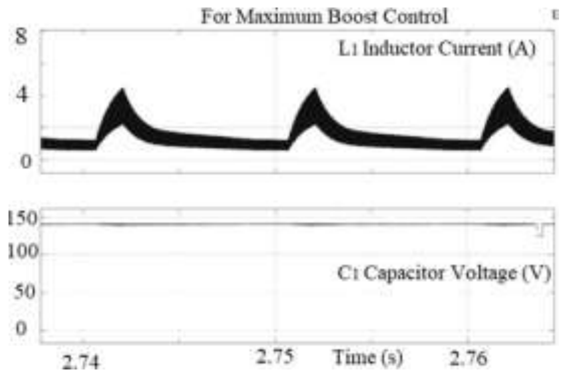

Fig. 17. Ripple SL-qZSI inductor current and capacitor voltage for MBC

Neuro Quantology | September 2022 | Volume 20 | Issue 9 | Page 4715-4726 | doi: 10.14704/nq.2022.20.9.NQ44547

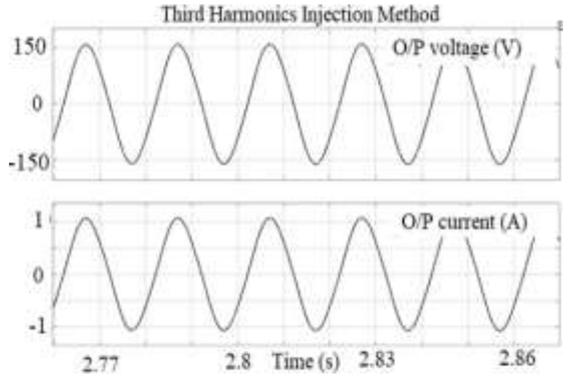

Fig. 18. Load voltage and current for THI- ripple SL-qZSI

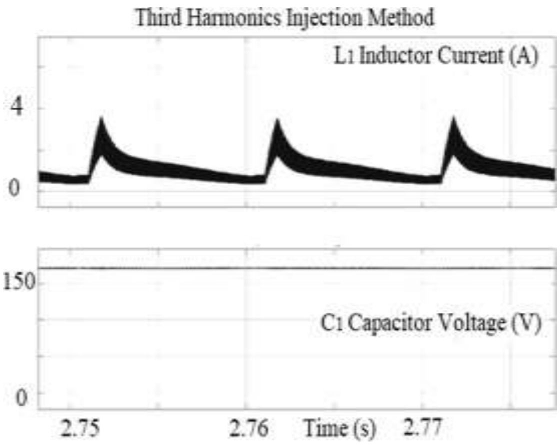

Fig. 19. Ripple SL-qZSI inductor current and capacitor voltage for THI control.

The output voltage of ripple SL-qZSI with Third Harmonic Injection (THI) control for modulation control 0.9 is shown in the Fig. 18. A peak voltage of 154V with 1.08A are observed. Beside that, in Fig. 19, the current through the inductor (L_1) and capacitor voltage (C_1) are shown. A peak value near 4Amp with maximum ripple of 25% is observed. Similarly capaitor voltage (C_1) of 170V with very minimum ripple is also appeared.The voltage and current across the switch for this THI control are shown in Fig. 20.

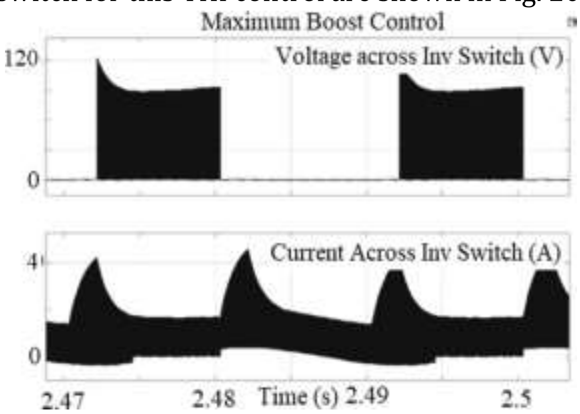

Fig. 20. Voltage and current across Ripple SL-qZSI switch.

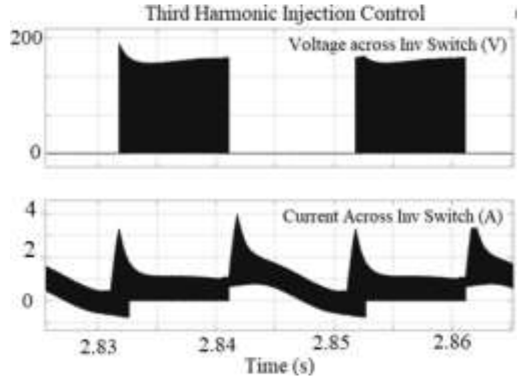

Fig. 21.Voltage and current across two SL- qZSI switch.

Table -2 Variation of Output Voltage and Current for different Modulation

Modulation Index	Maximum Boost Control (MBC)		Third Harmonic Injection (THI)	
	Output Voltage (V)	Output Current (A)	Output Voltage (V)	Output Current (A)
0.7	90	0.9	134	0.94
0.8	110	1.1	150	1.06
0.9	119	1.18	154	1.08
1	122	1.21	154	1.08
1.1	124	1.26	154	1.08

Effect of the variation of modulation index for both MBC and THI control is shown in table 2. Modulation index will varied from 0.7 to 1.1 and an output voltage variation from 90V to 122V is observed in MBC. For similar modulation index variation, a range of output voltage from 134V to 154V is noticed for THI control.

6. Conclusion:

In recent year qZSI type inverter structures are getting importance for different power level application. As, introduced earlier, different qZSI topologies are already prescribed by different researches. A comparative analysis, in terms of boost factor and voltage gain is given in table-2.

Table -2 Comparative analysis different ZSI

Topology	Boost Factor	Voltage Gain
SL-qZSI [22]	$B=\frac{1+D}{1-2D-D^2}$	$G=\frac{8\pi^2 M-6\sqrt{3}\pi M^2}{-8\pi^2+24\sqrt{3}\pi M-27M^2}$
SCL-qZSI [23]	$B=\frac{3}{(1-4D)}$	$G=\frac{3M}{4M-3}$
Enhanced BZSI [24]	$B=\frac{1}{2D^2-4D+1}$	$G=\frac{M}{2D^2-4D+1}$
TL-qZSI [25]	$B=\frac{1+D}{1-2D-D^2}$	$G=\frac{M[(1-M)+1]}{2M-N(1-M^2)-1}$
qZS-DMC [26]	$B=\frac{1}{\sqrt{3D^2-3D+1}}$	$G=\frac{M}{2M-1}$
ASC/SL-qZSI [27]	$B=\frac{1+D}{1-3D}$	$G=\frac{M(4-\sqrt{3}M)}{3\sqrt{3}M-4}$
Ripple SL-qZSI	$B=\frac{1+D}{1-3D}$	$G=\frac{2M-M^2}{3M-2}$

In this paper a two stage, i.e. a dc boost converter and a ripple SL-qZSI based renewable energy system is proposed. For maximum power extraction an incremental conductance based MPPT control technique is also used in this proposed work. Two different qZSI boost control methods, MBC and THI control with different modulation index from 0.7 to 1.1, are also implemented. The total system is designed in MATLAB software and verification of different current and voltage characteristics are successfully executed.

Reference

L. Hernández-Callejo, S. Gallardo-Saavedra, and V. Alonso-Gómez, "A review of photovoltaic systems: Design, operation and maintenance," Solar Energy, vol. 188, no. March, pp. 426–440, 2019, doi: 10.1016/j.solener.2019.06.017.

S. Mukherjee, S. S. Saha, and S. Chowdhury, "Design of duty-ratio and phase-shift control circuits for MPPT of SPV Source using ZV-ZCS PSFB Converters," in Proceedings of 4th International Conference on 2021 Devices for Integrated Circuit, DevIC 2021, 2021, pp. 555–559, doi: 10.1109/DevIC50843.2021.9455893.

H. Aboreada, A. V. J. S. Praneeth, N. Vamanan, V. Sood, and S. S. Williamson, "Design and Control of Non-isolated, Multi-input DC/DC Converter for Effective Energy Management," IEEE International Symposium on Industrial Electronics, vol. 2019-June, pp. 810–815, 2019, doi: 10.1109/ISIE.2019.8781350.

D. Banerjee, S. Mukherjee, and R. Dhar, Inverter with MPPT Technique. Springer Singapore, 2021.

T. Bang and J. W. Park, "Development of a ZVT-PWM buck cascaded buck-boost PFC converter of 2kW with the widest range of input voltage," IEEE Transactions on Industrial Electronics, vol. 65, no. 3, pp. 2090–2099, 2018, doi: 10.1109/TIE.2017.2739703.

T. F. Wu, Y. S. Lai, J. C. Hung, and Y. M. Chen, "Boost converter with coupled inductors and buck-boost type of active clamp," IEEE Transactions on Industrial Electronics, vol. 55, no. 1, pp. 154–162, 2008, doi: 10.1109/TIE.2007.903925.

A. Sadhukhan, S. S. Saha, A. Majumdar, and B. Majumdar, "An extended voltage gain buck-boost converter for maximum photovoltaic power extraction," International Journal of Electronics, vol. 00, no. 00, pp. 1–20, 2021, doi: 10.1080/00207217.2020.1870744.

C. H. Chang, E. C. Chang, C. A. Cheng, and C. L. Shen, "A step-up/down inverter implemented with the boost-interleaved buck-boost dc-dc converter," 2015, doi: 10.1109/IFEEC.2015.7361480.

J. Anderson and F. Z. Peng, "Four quasi-Z-Source inverters," PESC Record - IEEE Annual Power Electronics Specialists Conference, pp. 2743–2749, 2008, doi: 10.1109/PESC.2008.4592360.

F. Gao, P. C. Loh, D. Li, and F. Blaabjerg, "Asymmetrical and symmetrical embedded Z-source inverters," IET Power Electronics, vol. 4, no. 2, pp. 181–193, 2011, doi: 10.1049/iet-pel.2009.0213.

Y. P. Siwakoti, F. Z. Peng, F. Blaabjerg, P. C. Loh, and G. E. Town, "Impedance-source networks for electric power conversion Part I: A topological review," IEEE Transactions on Power Electronics, vol. 30, no. 2, pp. 699–716, 2015, doi: 10.1109/TPEL.2014.2313746.

V. Jagan, J. Kotturu, and S. Das, "Enhanced-Boost Quasi-Z-Source Inverters with Two-Switched Impedance Networks," IEEE Transactions on Industrial Electronics, vol. 64, no. 9, pp. 6885–6897, 2017, doi: 10.1109/TIE.2017.2688964.

X. Fang, B. Ma, G. Gao, and L. Gao, "Three Phase Trans-Quasi-Z-Source Inverter," CPSS Transactions on Power Electronics and Applications, vol. 3, no. 3, pp. 223–231, 2018, doi: 10.24295/cpsstpea.2018.00022.

A. K. Podder, N. K. Roy, and H. R. Pota, "MPPT methods for solar PV systems: A critical review based on tracking nature," IET Renewable Power Generation, vol. 13, no. 10, pp. 1615–1632, 2019, doi: 10.1049/iet-rpg.2018.5946.

D. Sera, L. Mathe, T. Kerekes, S. V. Spataru, and R. Teodorescu, "On the perturb-and-observe and incremental conductance mppt methods for PV systems," IEEE Journal of Photovoltaics, vol. 3, no. 3, pp. 1070–1078, 2013, doi: 10.1109/JPHOTOV.2013.2261118.

A. Ilyas, M. Ayyub, M. R. Khan, A. Jain, and M. A. Husain, "Realisation of incremental conductance the MPPT algorithm for a solar photovoltaic system," International Journal of Ambient Energy, vol. 39, no. 8, pp. 873–884, 2018, doi: 10.1080/01430750.2017.1354322.

J. K. Shiau, Y. C. Wei, and B. C. Chen, "A study on the fuzzy-logic-based solar power MPPT algorithms using different fuzzy input variables," Algorithms, vol. 8, no. 2, pp. 100–127, 2015, doi: 10.3390/a8020100.

S. Mukherjee, "MUKHERJEE A SEPIC-CUK-CSCCC BASED SIMO CONVERTER DESIGN USING PSO-MPPT FOR RENEWABLE ENERGY APPLICATION," no. Ic, pp. 111–117, 2021.

A. P. Podey and J. O. Chandle, "Stability Analysis of DC-DC Boost Converter using Sliding Mode Controller," 2020 IEEE PES/IAS PowerAfrica, PowerAfrica 2020, 2020, doi: 10.1109/PowerAfrica49420.2020.9219954.

X. Fang, "Maximum boost control of the current-fed Z-source inverter," Proceedings of the IEEE International Conference on Industrial Technology, no. I, pp. 255–260, 2008, doi: 10.1109/ICIT.2008.4608348.

S. DebBarman and T. Roy, "Different Types of PWM Techniques analysis for Z-Source Inverter," IOSR Journal of Electrical and Electronics Engineering, vol. 9, no. 3, pp. 09–17, 2014, doi: 10.9790/1676-09340917.

W. Qian, F. Z. Peng, and H. Cha, "Trans-Z-Source Inverters," vol. 26, no. 12, pp. 3453–3463, 2011.

B. Axelrod, Y. Berkovich, and A. Ioinovici, "Switched-capacitor/switched-inductor structures for getting transformerless hybrid DC-DC PWM converters," IEEE Transactions on Circuits and Systems I: Regular Papers, vol. 55, no. 2, pp. 687–696, 2008, doi: 10.1109/TCSI.2008.916403.

H. Fathi and H. Madadi, "Enhanced-Boost Z-Source Inverters with Switched Z-Impedance," IEEE Transactions on Industrial Electronics, vol. 63, no. 2, pp. 691–703, 2016, doi: 10.1109/TIE.2015.2477346.

Y. Zhou, W. Huang, J. Zhao, and P. Zhao, "Tapped inductor quasi-Z-source inverters," Zhongguo Dianji Gongcheng Xuebao/Proceedings of the Chinese Society of Electrical Engineering, vol. 32, no. 27, pp. 126–134, 2012.

F. Z. Peng and S. Member, "Z-Source Inverter," vol. 39, no. 2, pp. 504–510, 2003.

Q. Lei, D. Cao, and F. Z. Peng, "Novel loss and harmonic minimized vector modulation for a current-fed quasi-Z-source inverter in HEV motor drive application," IEEE Transactions on Power Electronics, vol. 29, no. 3, pp. 1344–1357, 2014, doi: 10.1109/TPEL.2013.2260173.